Effect of Nd-Rich Phases on the Corrosion Behavior of AZ80 Magnesium Alloy in Alkaline Solution

QI ZOU [iD],[1] QICHI LE,[1] XINGRUI CHEN,[1] CHUNYAN BAN,[1,2]
YONGHUI JIA,[1] RUIZHEN GUO,[1] and AN WANG[1]

1.—Key Lab of Electromagnetic Processing of Materials, Ministry of Education, Northeastern
University, Shenyang, Liaoning 110819, People's Republic of China. 2.—e-mail: bancy@epm.neu.edu.cn

This work investigated the corrosion resistance of AZ80 (Mg-8Al-0.5Zn alloy)
with different Nd contents in alkaline solution by the mass loss test, electro-
chemical test, scanning electron microscope, energy spectrum analysis, and x-
ray diffraction. To remove the influence of the $Mg_{17}Al_{12}$ phase, alloys were
heat treated at 410°C for 10 h. Results revealed that Al_2Nd and AlMnNd
phases mainly exist in the alloy. The corrosion rate of the alloy increased when
the Nd content was < 0.4 wt.% because the Al_2Nd phase formed galvanic
corrosion with the Mg matrix. With the increase of Nd content, AlMnNd phase
appeared in the alloys, which decomposed during the corrosion process and
formed a good protective film to reduce the corrosion rate.

INTRODUCTION

Magnesium alloys have become a promising raw
material for the construction industry due to their
advantages of low density, high strength-to-weight
ratio, good shock absorption performance, rich
resources, and easy recycling, which are compatible
with the modern concept of green, energy-saving,
and environmental protection.[1] However, the poor
corrosion resistance of magnesium alloys restricts
its wide application. Researchers have proposed
many methods to improve the corrosion resistance
of Mg alloys, such as surface coating technologies,
surface treatment technologies, and alloying.[2–4]
Surface treatment methods including chemical con-
version coating, electrodeposition, organic coating,
and plasma electrolyte oxidation (PEO) process
have been extensively studied.[5–7] Nevertheless,
the surface treatment and surface coating technolo-
gies may be restricted by environmental conditions,
and the preparation technologies are complicated.[8]
Alloying technology has attracted increasing atten-
tion because it can improve the inherent corrosion
resistance of alloys and has advantages of high
feasibility and low cost.[9] Although alloying may
increase impurities, the effects of impurities can be

reduced by using high-purity raw materials and
special preparation processes.[10] In addition, alloy-
ing technology can change the phase structure,
improve the thermodynamic stability of the mate-
rial, and enhance the passivation ability of the
material by forming a surface protective film,
thereby reducing the corrosion rate of Mg alloys.[11]

Mg-Al-based alloys are the most widely used
magnesium alloys because they exhibit excellent
mechanical properties and corrosion resistance.[12]
Nordlien et al.[13] proposed that the Al-rich substrate
can improve the corrosion resistance since the
significant enrichment of the aluminum oxide
increases the stability of the passive film. The
corrosion rate of Mg-Al alloys decreases with the
increase of aluminum amounts,[14] which generally
depends on the amount and distribution of the β-
$Mg_{17}Al_{12}$ phase. Since the β-$Mg_{17}Al_{12}$ phase has a
more positive potential than the Mg matrix, the
discontinuous island β-phase accelerates corrosion
progress, while the continuous β-phase protects the
matrix from corrosion.[15–17]

In recent years, many researchers have found
that adding rare earth (RE) elements into the Mg-
Al-based alloys can effectively improve the corrosion
resistance of magnesium alloys.[18–21] RE elements
combine with the impurities to form intermetallic
compounds, which reduce the electrical effects and
promote the formation of the oxide film in $Mg(OH)_2$
lattice.[22,23] As a RE element, Nd has been studied

for the alloying of magnesium alloys.[24] For instance, Zhang et al.[25] found that Nd increased the percent of the non-Faraday process and led to the anisotropy feature on the corrosion mechanism. The total corrosion weight loss included Faraday and non-Faraday weight loss. The non-Faraday process percentages of extruded AZ91 + 1.5Nd alloy were different on the transversal section and the longitudinal section, because the transversal section was mainly dominated by the generation of intermediate Mg^+, while the longitudinal section was controlled by the fall off of the Al_3Nd phase. Su et al.[26] reported that AZ80-0.6Nd alloy exhibited better mechanical properties than AZ80 magnesium alloy, and the tensile strength, yield strength, and elongation of AZ80-0.6Nd alloy were increased 25%, 31.6%, and 47.5%, respectively, compared to AZ80. Zhang et al.[27] found that the addition of Nd can improve the corrosion resistance of AM60 alloy, for example, the corrosion rate decreased from 9.38 to 3.95 mg cm$^{-2}\cdot$d^{-1} in 3.5 wt.% NaCl solution when the Nd content was 0.9%.

Magnesium alloys have the potential to be used as building formwork in the construction industry to achieve lightweight and green construction, which means that magnesium alloys need to be exposed to cement concrete environments. The corrosion behavior of steel in cement concrete has been investigated.[28,29] Currently, the studies on the corrosion behaviors of magnesium alloys mainly focused on acidic and neutral (e.g., NaCl aqueous solution) environments.[30] However, the corrosion resistance of magnesium alloys in alkaline environments (such as cement concrete, alkaline soil) has not been investigated. Therefore, it is of great significance to study the corrosion resistance of magnesium alloys in alkaline environments to expand its application range. In this work, the corrosion behavior of AZ80-xNd alloys in a simulated alkaline cement environment was investigated. The effects of the Nd-rich phases on the microstructure and corrosion behavior of AZ80 magnesium alloy in the alkaline environment were studied. The feasibility of the improved alkali resistance of AZ80 magnesium alloy via Nd alloying and the optimal Nd content was explored.

EXPERIMENTAL METHODS

Test Materials and Specimen Preparation

Four alloys with different Nd contents were prepared, and their compositions are listed in Table SI. The raw materials used in this experiment included commercially pure magnesium (99.99 wt.%), high-purity aluminum (99.99 wt.%), pure zinc (99.99 wt.%), $MnCl_2$ particles, and Mg-22.4 wt.% Nd master alloy, supplied by Baotou Research Institute of Rare Earth (Baotou, China). First, commercially pure Mg was melted in a graphite crucible at 710°C under the protective atmosphere of argon gas. Second, pure Al, pure Zn

and Mg-Nd master alloys were put into the crucible at 720°C, and then $MnCl_2$ particles were added to the melted alloy after 20 min for melt homogenization. The melt was poured into a water-cooling copper mold with a size of 200 mm × 200 mm × 80 mm at 690°C. Four basic alloys with different Nd contents were produced. These four as-cast basic alloys were heat-treated (410°C × 10 h) to eliminate the β-$Mg_{17}Al_{12}$ phase and cooled in the air. The four test ingots named AZ80-0.4Nd (Mg-8Al-0.5Zn-0.4Nd), AZ80-0.8Nd (Mg-8Al-0.5Zn-0.8Nd), AZ80-1.2Nd (Mg-8Al-0.5Zn-1.2Nd) and AZ80-1.6Nd (Mg-8Al-0.5Zn-1.6Nd) were obtained.

Immersion and Mass Loss Test

To investigate the corrosion performance of alloys, specimens were cut into coupons with the dimensions of 15 mm × 15 mm × 5 mm. More than three duplicate samples were used to ensure accuracy. The Na_2SiO_3 solution was selected as the simulation solution that could effectively simulate the building environment. Samples were immersed in 0.1 mol/L Na_2SiO_3 solutions at the pH of 8.5 and 12, respectively. The scheme of two pHs was employed to simulate the different alkalinity of building cement. The concentrated sulfuric acid was used to adjust the pH considering the addition of calcium sulfate to adjust the setting time during cement production. The corrosive solution was updated every 8 h to keep the pH stable. After immersion for 24 h at room temperature (25°C), the corroded specimens were washed in a chromate acid solution containing 200 g/L CrO_3, 20 g/L $Ba(NO_3)_2$, and 10 g/L $AgNO_3$ for 5–10 min to remove the corrosion products.[11] All chemicals were analytical grade and purchased from Aladdin. After cleaning, specimens were washed with deionized water, dried by hot air flow, and reweighed to obtain weight loss.

Microstructure Observation

All specimens were wet ground with 2000 grit abrasive paper and etched in an acetic-nitric reagent (1 g oxalic acid + 1 mL acetic acid + 1 mL nitric acid + 150 mL H_2O) for microstructure observation. After etching, morphological observation and element analysis were performed by scanning electron microscope (Zeiss ULTRA PLUS). For the samples after the immersion test, micro morphologies were observed by scanning electron microscope (Zeiss ULTRA PLUS). The 3D laser confocal microscope (OLYMPUS ols4100) was also used to measure the 3D morphology and surface roughness after corrosion. The constituent phases were identified by the x-ray diffractometer (X Pertpro) with scanning angle of 15°–85° and scanning time of 12 min. MDI Jade 6 software was used to analyze XRD peaks, and the software database was based on PDF2004.

Electrochemical Tests

Electrochemical experiments were carried out using a classic three-electrode cell system with an electrochemical workstation (ChenHua CHI660E). A platinum plate, a saturated calomel electrode (SCE), and the tested samples were employed as the counter electrode, reference electrode, and working electrode, respectively. The exposed area of tested samples was 1 cm^2. All samples were ground with SiC paper to 2000 grade and tested in Na$_2$SiO$_3$ solutions with different pH values at room temperature (25°C). The polarization curves were scanned from − 250 to + 250 mV relative to the open-circuit potential (OCP) with a scan rate of 1 mV/s after the sample was kept in the solution for 24 h. The electrochemical impedance spectroscopy (EIS) results were measured after the samples were held in the solution for 24 h to reach a stable value of the open-circuit potential (OCP). The scanned frequency ranged from 100 kHz to 0.1 Hz, and the voltage amplitude was 5 mV. To ensure reliability, at least five repetitions were made for each test. The ZSimpWin 3.20 software was used to analyze and fit the EIS spectrum.

RESULTS AND DISCUSSION

Microstructure

Figure S1 shows the microstructure of as-cast AZ80-0.4Nd alloy without heat treatment. Precipitated phases of β-Mg$_{17}$Al$_{12}$, Al$_2$Nd, and AlMnNd appeared and were distributed in the vicinity of grain boundaries. However, the overlapping phenomenon occurred between the β-phase and the Nd-rich phases, which could be due to the nucleation of β-phase at the location of Nd-rich intermetallics (Fig. S1b). To investigate the effect of Nd-rich phases on the corrosion resistance of alloys, the four basic alloys with different Nd contents were heat-treated at 410°C for 10 h to eliminate the β-phase.[31] It is worth mentioning that the lack of reinforcement of the β-phase may lead to a decrease in the mechanical properties of the alloy.

Figure 1 illustrates the microstructures of the four alloys with different Nd contents after heat treatment. The precipitated phases in the investigated alloys were Al$_2$Nd and AlMnNd phases. Figure S2 depicts the distribution of Nd in AZ80-1.2Nd alloy determined by EDS and element mapping. Since the difference in electronegativity between RE and Al was larger than that between RE and Mg, RE combined with Al to form Al-RE compounds preferentially.[32] Mg-RE intermetallic compounds were not formed in the alloys. Table SII lists the EDS results at different positions in Fig. 1. The heat treatment eliminated the β-Mg$_{17}$Al$_{12}$ phase but did not affect the rare earth phases because of the higher melting points of Al$_2$Nd and AlMnNd phases.[33] AZ80-0.4Nd alloy comprised the α-Mg matrix and rod-shaped Al$_2$Nd

phase (Fig. 1a and b). As the Nd content increased, the Al$_2$Nd phase in the alloy started to aggregate into a feather-like phase (Fig. 1f), which was similar to the results reported by Zhang et al.[34] Besides, the massive AlMnNd phase was observed in AZ80-1.2Nd and AZ80-1.6Nd alloys (Fig. 1f and h), while the AlMnNd phase was not found in AZ80-0.4Nd alloy. The addition of Nd consumed Mn element to form AlMnNd compounds. The Al$_8$Mn$_5$ and τ-AlMn phases can effectively refine the grains because they acted as the heterogeneous nucleation substrate.[35] With the increase of Nd content, the AlMnNd phase gradually grew, and the partially bulk AlMnNd phase had grown significantly into the massive phase with a clear regular appearance and long lath phase.

Figure 2 shows the XRD patterns of heat-treated AZ80-xNd alloys. The common phases of the four alloys included the α-Mg phase and Al$_2$Nd phase. With the increase of Nd content, AlMnNd phase gradually appeared in the alloy. The AlMnNd phase was not observed in AZ80-0.4Nd alloy, which was consistent with the SEM images. Due to the heat treatment, the β-Mg$_{17}$Al$_{12}$ phase was not found in four alloys, indicating that the Al element in β-phase was completely dissolved into the α-Mg matrix.[31]

Electrochemical Test

Figure 3 shows the polarization curves of AZ80-xNd alloys measured in Na$_2$SiO$_3$ solution with different pH values for 24 h. AZ80-1.6Nd and AZ80-1.2Nd alloys had the lowest corrosion potentials at pH 8.5 and 12, respectively. Generally, the corrosion potential of the alloys decreased with the increase of Nd. It should be noted that it is not reliable to only evaluate corrosion resistance based on the corrosion potential.[36] In the cathode branch, the cathode current density gradually decreased with the increase of Nd content to 1.2 wt.%. However, when the Nd content continuously increased to 1.6 wt.%, the cathode current density increased. Table SIII illustrates the detailed corrosion parameters fitted using Tafel extrapolation, including corrosion potentials (E_{corr}), corrosion current densities (i_{corr}), and polarization resistance (R_p). The Tafel region data selected for Tafel extrapolation were corrosion potentials (E_{corr}) $\pm$ 50–150 mV. Although the value of the corrosion current density cannot accurately represent the corrosion rate of most Mg alloys, it reflects the corrosion resistance qualitatively.[37] AZ80-1.2Nd alloy had the lowest corrosion current densities and the largest polarization resistance under the condition of two pH values, indicating that as the Nd content increased, the self-corrosion rate of the alloys reduced, but when the Nd content exceeded 1.2–1.6 wt.%, the self-corrosion rate increased. Nd-rich phases should respond to these results, and the detailed mechanism was discussed behind. It is important to note
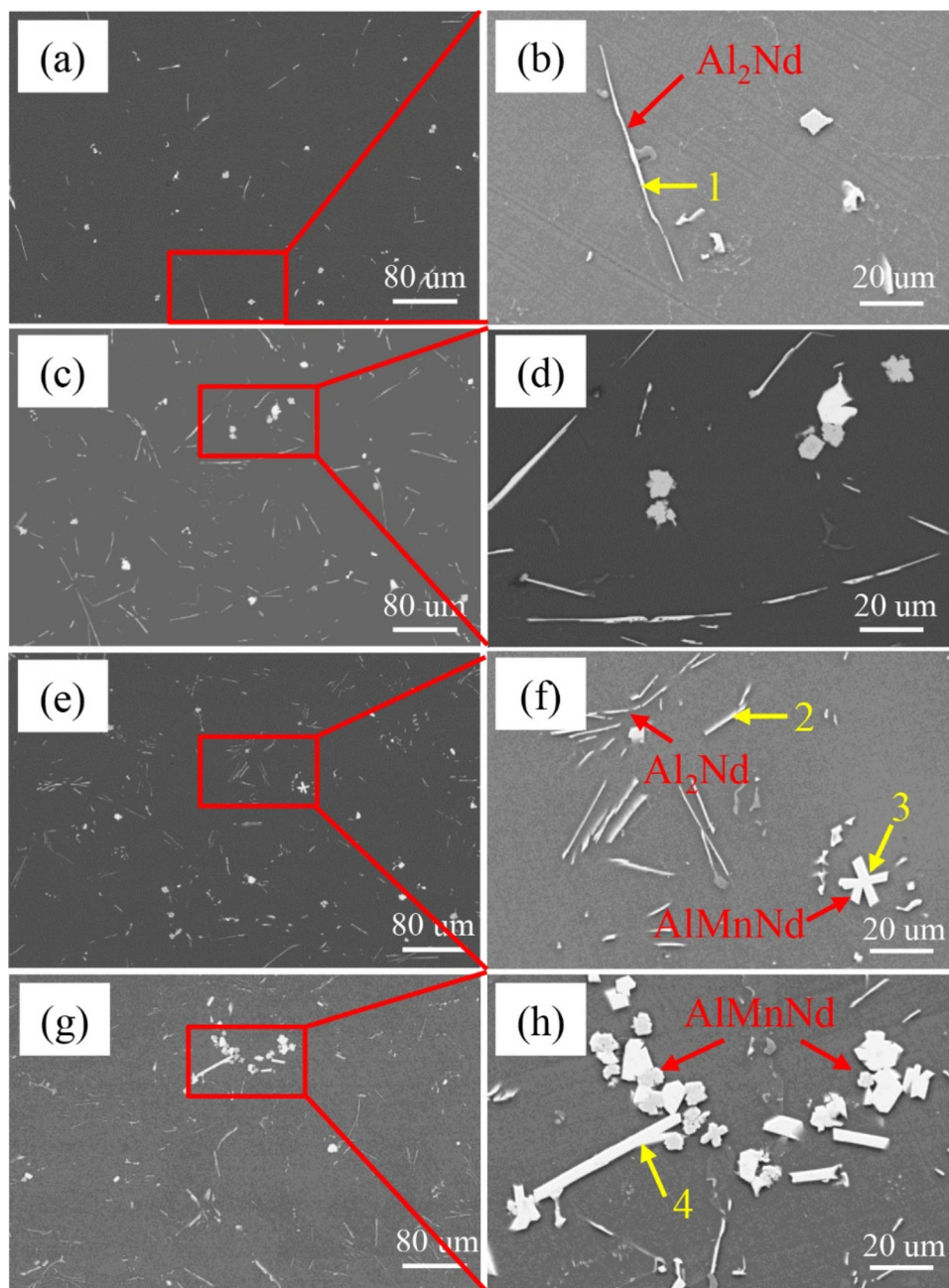
Fig. 1. SEM images of (a), (b) AZ80-0.4Nd, (c), (d) AZ80-0.8Nd, (e), (f) AZ80-1.2Nd, and (g), (h) AZ80-1.6Nd.

that the corrosion potentials of the four alloys in the corrosive solution at pH 12 were lower than those at pH 8.5, which means that AZ80-xNd alloys exhibited better corrosion resistance in the strongly alkaline solution. Tang et al.[38] found that AZ91 magnesium alloy presented better corrosion resistance in Na_2SO_4 solution at pH 12 compared to that at pH 9. On the one hand, as the alkalinity increased, the electrochemical activity of the alloy decreased. On the other hand, the morphologies of the corrosion products changed from white reticulated lines to a flocculated film.

Figure 4 presents the electrochemical impedance spectrum (EIS) of AZ80-xNd alloys exposed to the Na_2SiO_3 solutions at different pH values for 24 h. Impedance spectra contain experimental data (symbols) and theoretical fitting curves (lines), which simulated the experimental results employing equivalent electrical circuits. In general, the Nyquist spectra were similar except for the difference in the diameters of the loops according to the Nyquist plots (Fig. 4a and c). The electrochemical impedance spectrum of AZ80-xNd alloys consisted of two capacitive loops, one at high frequencies and the other at low frequencies. Each of the four

investigated alloys had a broad peak (as shown in Fig. 4b and d), which was due to the relatively close time constants with overlapping adjacent peaks. These two peaks correspond to the two corrosion processes in alloys since each corrosion reaction responded to voltage disturbances at different frequencies.[39] The high-frequency capacitance loop was concerned with the electron transfer of the oxidation reaction of the electrode, and the low-frequency capacitance loop related to the interface between the electrode and the solution.[5,40]

Figure 4e and f shows the equivalent circuit of the four alloys in alkaline solutions with pH 8.5 and 12, respectively. R_S was the solution resistance. R_f represented the film resistance, which was also related to the film porosity and the solution conductivity in the film pores, and the CPE_f was the film capacitance. R_t was the pseudo-resistance applied to de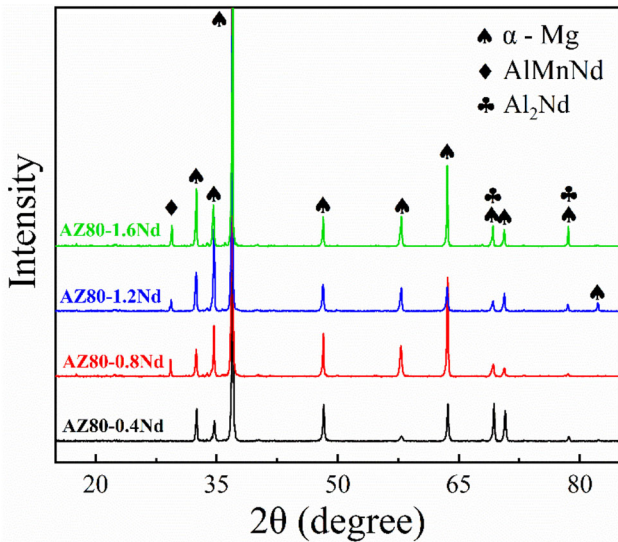scribe the electrochemical reactions at the film/Mg interface, and CPE_{dl} was the pseudo-capacitance. Two consecutive groups of the paralleled combination of resistor (R_f and R_t) and constant phase element (CPE_f and CPE_{dl}) corresponded to resistive parameters and capacitive of the outer and inner corrosion layer, respectively.[41] The EIS spectrum was analyzed and fitted using ZSimpWin 3.20 software, and the fitting results are listed in Table SIV. The R_f value increased and then decreased with the increase of Nd, with an inflection point of 1.2 wt.%. The R_f of AZ80-1.2Nd alloy reached the maximum value in two corrosive solutions with different pH values. In addition, the AZ80-1.2Nd alloy had the greatest value of the impedance modulus |Z|. The EIS results were consistent with the polarization curve results.

Corrosion Behavior in Immersion Testing

Figure S3 shows the mass-loss rates of the tested alloys in the immersion test. The mass-loss rates decreased first and then increased with the increase of Nd. In general, AZ80-1.2Nd had a lower weight loss rate than other alloys in the alkaline solution at pH 8.5 after immersion for 10 h, 24 h, and 48 h, and the corrosion rates were 0.053 ± 0.037 mg/cm^2 h^{-1}, 0.141 ± 0.030 mg/cm^2 h^{-1}, and 0.150 ± 0.070 mg/cm^2 h^{-1}, respectively. The mass-loss rate of AZ80-0.4Nd alloy was higher than that of the other three alloys. As the corrosion time extended, the corrosion rate of AZ80-0.4Nd alloy increased rapidly. The corrosion rate decreased with the increase of Nd content when the Nd content was below 1.2 wt.%. However, a further increase of Nd content to 1.6 wt.% expedited the corrosion rate.

The corrosion surfaces of AZ80-xNd alloys after immersion in the alkaline solution at pH 8.5 for 24 h are shown in Fig. 5. Table SV lists the EDS results at different positions (Fig. 5), and the results could identify the phases on the corroded alloys. Obvious traces of pitting corrosion were observed on the surface of AZ80-0.4Nd alloy (Fig. 5a), and needle-like bright phases were found in the center of the

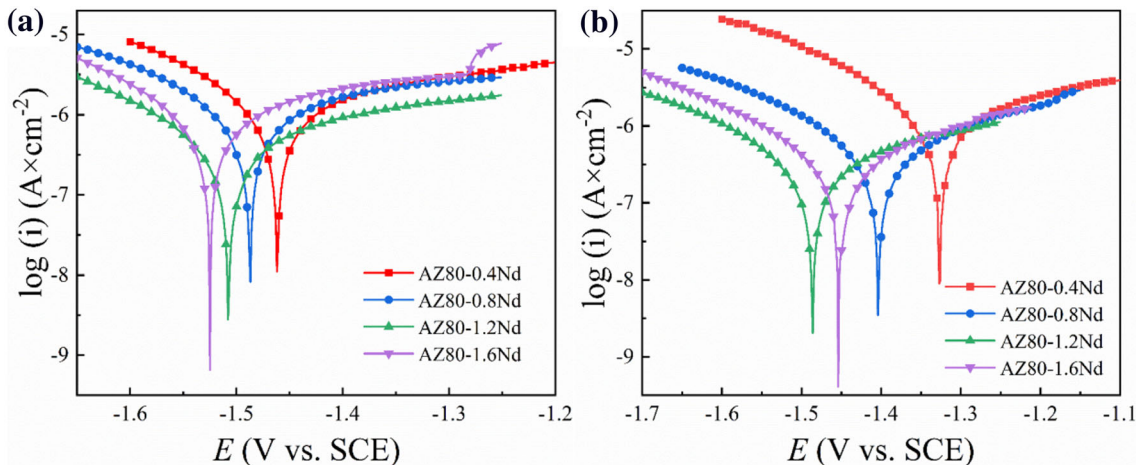Fig. 2. X-ray diffraction patterns of investigated alloys.

Fig. 3. Polarization curves of investigated alloys after immersion in alkaline solutions at (a) pH 8.5 and (b) pH 12 for 24 h.
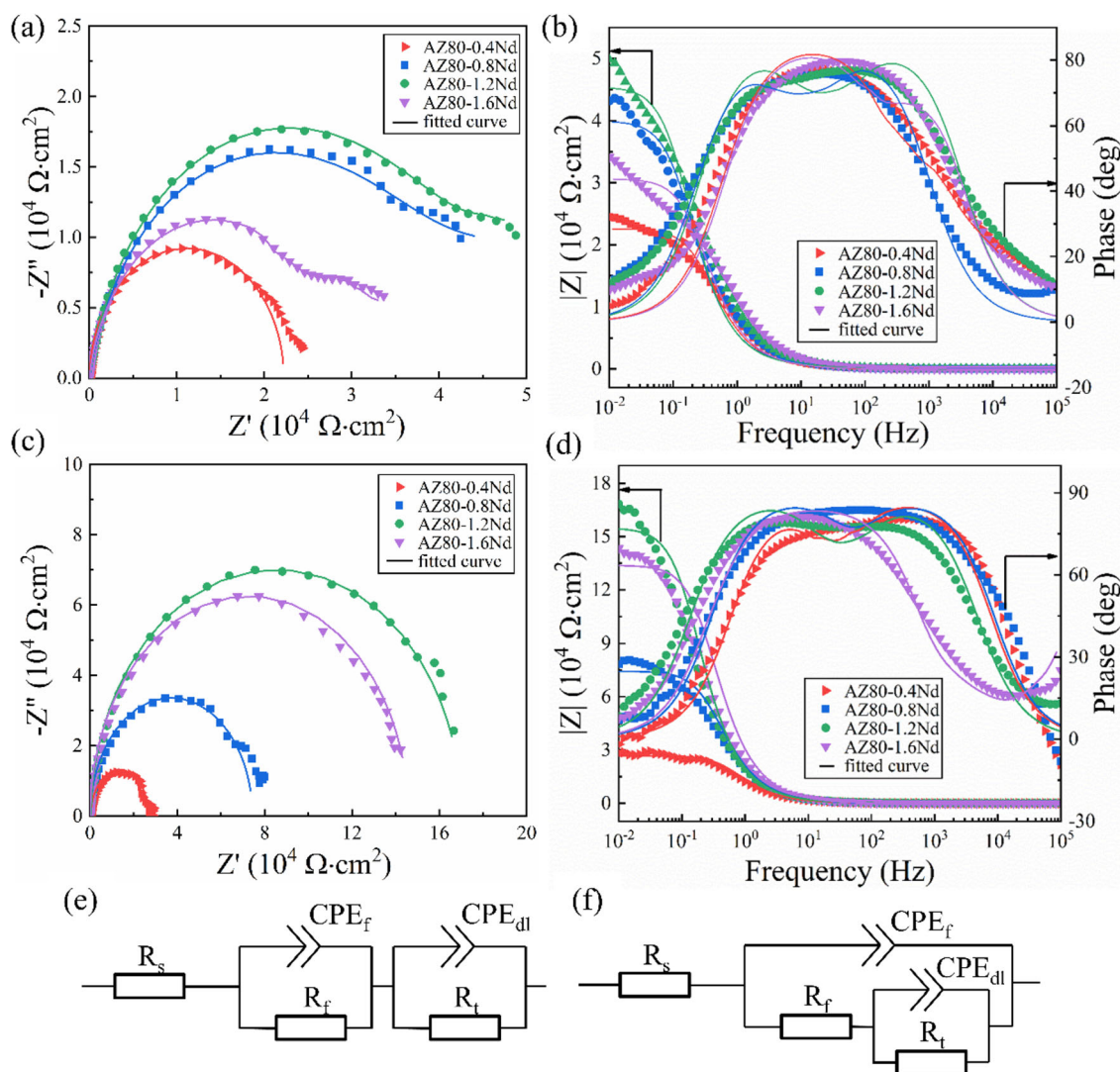
Fig. 4. Electrochemical impedance spectra (EIS) of investigated alloys: (a) Nyquist plots (pH 8.5); (b) Bode impedance and phase angle plots (pH 8.5); (c) Nyquist plots (pH 12); (d) Bode impedance and phase angle plots (pH 12); (e, f) equivalent circuits used for fitting the EIS.

pitting locations at high magnification (Fig. 5c). These needle-like phases can be identified as the Al_2Nd phase according to the structural analysis and the binding energy spectrum, indicating that the Al_2Nd phase had no morphological changes after corrosion. The potential of the Al_2Nd phase was more positive than that of the Mg matrix;[42] thus, the Al_2Nd phase accelerated the corrosion of the matrix, resulting in a large area of pitting corrosion.[43] Figure 5d shows that a large amount of pitting existed on the surface of AZ80-0.8Nd alloy. However, the corrosion area was generally less than that of AZ80-0.4Nd alloy. Both rod-shaped Al_2Nd phase and the bulk AlMnNd phase existed in corrosion pits on the surface of AZ80-0.8Nd alloy, while the AlMnNd phase tended to gradually decompose, which was different from the block shape before immersion. The decomposition of the AlMnNd phase formed a protective film on the surface of the alloys, which inhibited the galvanic

corrosion of the Nd-rich phases and α-Mg matrix. Similarly, Unocic et al.[44] found that Nd-rich phases decomposed during the corrosion process and formed a protective film to hinder the continuation of the corrosion reaction. Therefore, AZ80-0.8Nd alloy had better corrosion resistance than AZ80-0.4Nd alloy. Besides, a large amount of bright white debris was found on the surface, which was the decomposition product of the AlMnNd phase. The corrosion area enlarged with the increase of the RE phase, but the decomposition of the AlMnNd phase inhibited further corrosion. Combined with the two factors, when the Nd content increased to 1.2 wt.%, the AZ80-1.2Nd alloy exhibited the best corrosion resistance among the four tested alloys. However, when the Nd content further increased to 1.6 wt.%, many corrosion grooves and deeper pitting pits appeared, indicating that the higher Nd content could accelerate corrosion.
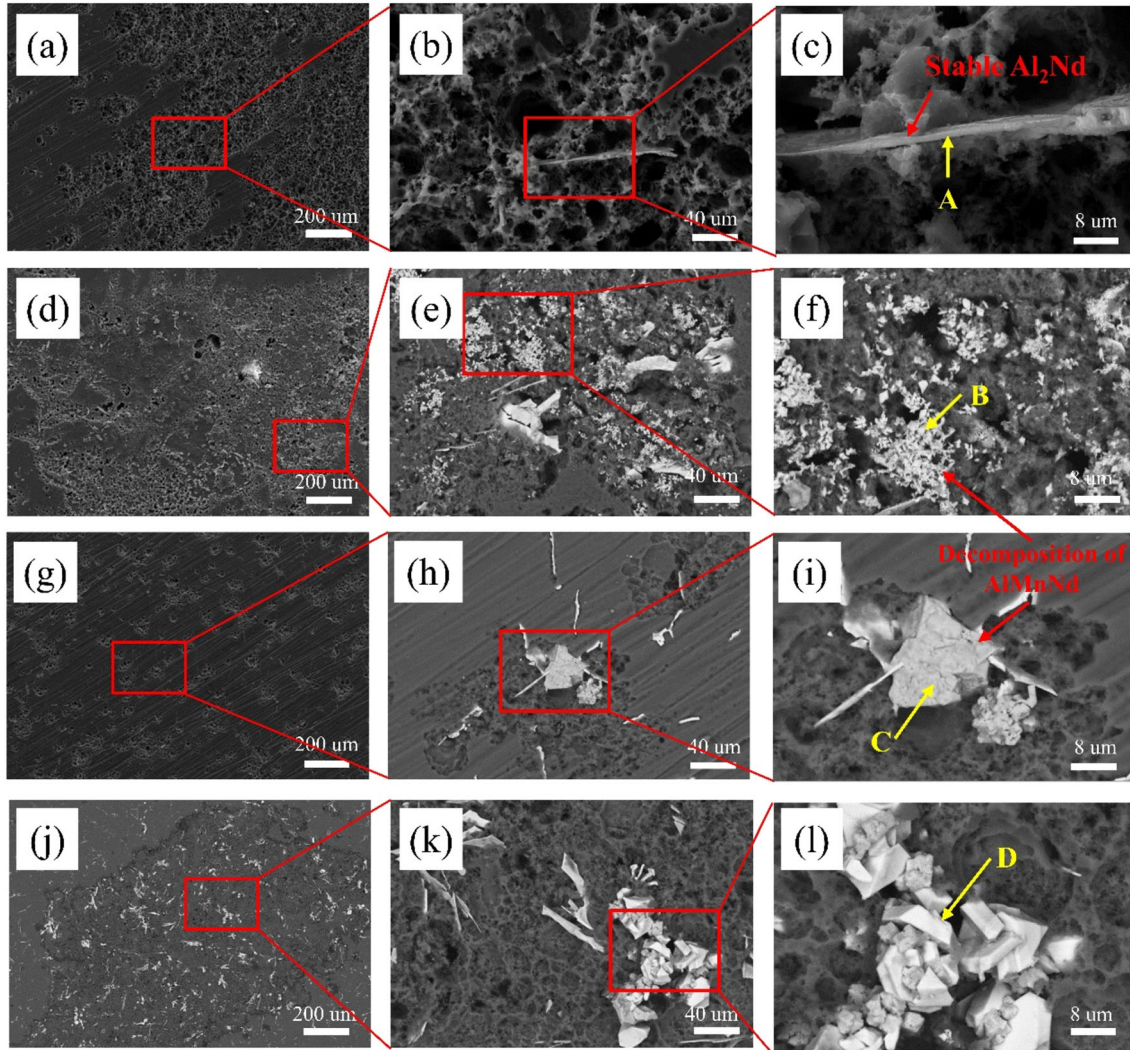
Fig. 5. Surface morphologies of (a)–(c) AZ80-0.4Nd, (d)–(f) AZ80-0.8Nd, (g)–(i) AZ80-1.2Nd, and (j)–(l) AZ80-1.6Nd after immersion in alkaline solution (pH 8.5) for 24 h.

Figure 6 shows 3D CLSM images, line morphologies, and surface roughness of investigated alloys after immersion in alkaline solution (pH 8.5) for 24 h. The 3D CLSM images directly depict the macroscopic morphology and the depth of corrosion pits. The maximum depth of corrosion pits of AZ80-0.4Nd, AZ80-0.8Nd, AZ80-1.2Nd, amd AZ80-1.6Nd alloys were 136.94 μm, 134.86 μm, 135.16 μm, and 122.134 μm, respectively. As shown in Fig. 6a, b, c, and d, the depth of corrosion increased with the increase of Nd content when the Nd content was < 1.2 wt.%. When the Nd content was added to 1.6 wt.%, many corrosion areas appeared on the surface of the AZ80-1.6Nd alloy. To further reflect the corrosion resistance of the four alloys, the line morphology and surface roughness (Ra) of AZ80-xNd alloys were investigated after immersion in the corrosive solution at pH 8.5 for 24 h (Fig. 6e). AZ80-1.2Nd alloy had the flattest line morphology and the

lowest surface roughness. Furthermore, the surface roughness of investigated alloys decreased and then increased with the increase of Nd content, with an inflection point of 1.2 wt.%.

Since the corrosion rates of the four alloys in the alkaline solution (pH 12) were very slow, only AZ80-0.4Nd alloy with the fastest corrosion rate and AZ80-1.2Nd alloy with the slowest corrosion rate were selected to observe the surface morphology, as shown in Fig. 7. Many deep corrosion pits were observed on the surface of AZ80-0.4Nd alloy, while the number of corrosion pits on the surface of AZ80-1.2Nd alloy was relatively small. The white debris that appeared on AZ80-1.2Nd alloy could be regarded as the protective film produced by the decomposition of the AlMnNd phase, and this phenomenon was similar to that in Fig. 5h and j. The mass loss results are given in Fig. 7g; the corrosion rate of AZ80-1.2Nd alloy was the lowest.
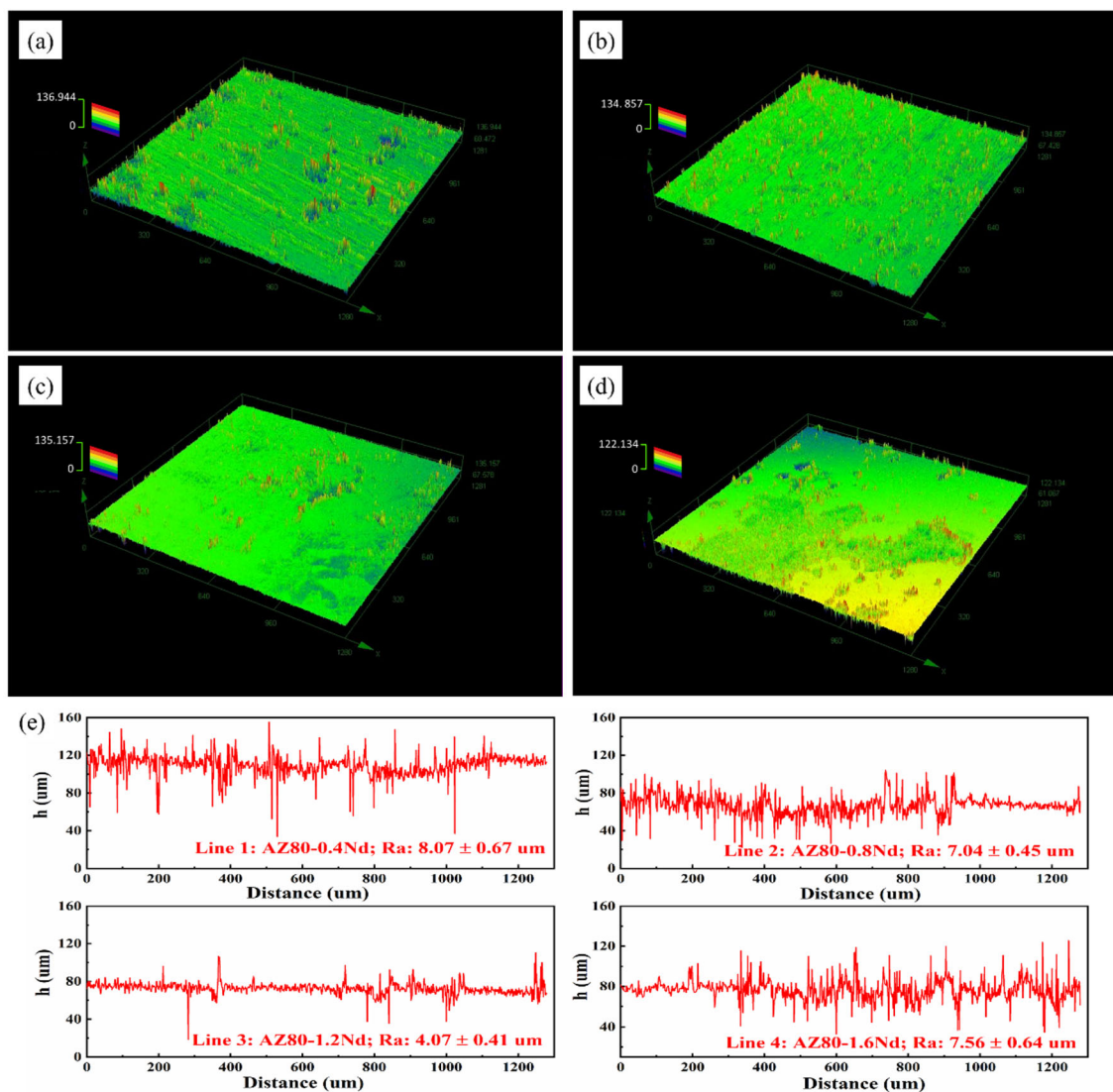
Fig. 6. Three-dimensional CLSM images of (a) AZ80-0.4Nd, (b) AZ80-0.8Nd, (c) AZ80-1.2Nd, amd (d) AZ80-1.6Nd alloys. (e) Line morphologies and surface roughness after immersion in alkaline solution at pH 8.5 for 24 h.

Besides, within the same immersion time of 24 h, the corrosion rates of the AZ80-xNd alloys were lower at pH 12 than that at pH 8.5, which means that the AZ80-xNd alloys had better corrosion resistance in strongly alkaline solution.

The Nd content significantly affects the corrosion performances of the AZ80-xNd alloys, and the Nd precipitations hold the key. The potentials of the Al_2Nd phase and AlMnNd phase were 15–45 mV and 75–110 mV, respectively, which were higher than the potentials of the α-Mg matrix.[43] Therefore, both Al_2Nd and AlMnNd phases can build galvanic couples with the Mg matrix and promote the corrosion process. In fact, the surface film of magnesium alloys was multilayered. Esmaily et al.[45] proposed that the corrosion film of the Mg-Al alloy consisted of an inner layer rich in Mg oxide and an outer columnar mixed Mg oxide-hydroxide layer on top. However, the hydroxide layer was discontinuous and only partially covered the surface of the alloy, which cannot effectively protect the surface of the alloy.[46,47] Therefore, the decomposition of the Nd-rich phases played a key role in the corrosion process.

To better explain the influence of Nd-rich phases on the corrosion resistance, the schematic of the corrosion process is shown in Fig. 8. When the Nd content was 0.4 wt.%, galvanic corrosion occurred around the Al_2Nd phase to accelerate the corrosion of the alloys (Fig. 8a). When the Nd content increased, the AlMnNd phase appeared in the alloys (i.e., AZ80-0.8, 1.2, and 1.6 Nd), which exhibited a
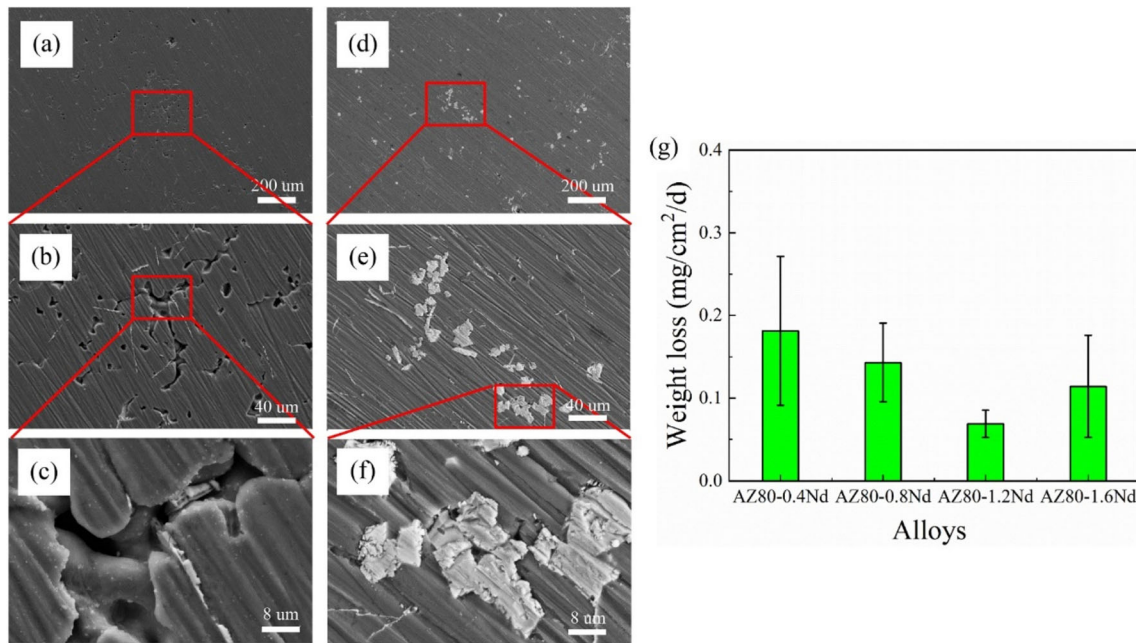
Fig. 7. Surface morphologies of (a)–(c) AZ80-0.4Nd and (d)–(f) AZ80-1.2Nd; (g) Mass-loss results of investigated alloys after immersion in the alkaline solution at pH 12 for 24 h.

lower corrosion rate than AZ80-0.4Nd, since the product from the decomposition of AlMnNd phase provided a protective film to protect the Mg matrix from corrosion. Therefore, the two mechanisms of the AlMnNd phase competed with each other to influence the corrosion process. In the weak alkaline solution (i.e., pH 8.5), the corrosion rate decreased and then increased with the increase of Nd, resulting in AZ80-1.2Nd alloy having the best corrosion resistance among the four alloys. The increased volume fraction of the AlMnNd phase improves the corrosion resistance because of the enhanced protective film (Fig. 8b). However, further increase of Nd content to 1.6 wt.% led to more AlMnNd phase in the matrix, which obtained worse galvanic corrosion and resulted in the degradation of corrosion performance (Fig. 8c).

In the strong alkaline solution (i.e., pH 12), the corrosion rates of four alloys were significantly reduced according to the results of the mass-loss rates and the electrochemical tests. When the pH value was 12, a lot of SiO_3^{2-} and SO_4^{2-} was in the solution because of the concentrated sulfuric acid used to adjust the pH value of the corrosive solution. Sodium silicate can greatly improve the corrosion resistance of the anode film.[48] With the increase of pH, Al^{3+} also reacted with the eutectic magnesium phases and generated $MgAl_2(SO_4)_4 \cdot 2H_2O$ precipitation (Eq. 1).[49] The increase of SO_4^{2-} content in the strong alkali solution promoted the formation of

precipitates, thereby suppressing further progress of corrosion.

$$Mg + 2Al^{3+} + 4SO_4^{2-} + 2H_2O \rightarrow MgAl_2(SO_4)_4 \cdot 2H_2O + 2e^- \qquad (1)$$
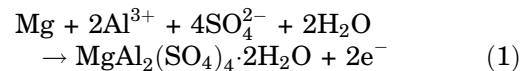
CONCLUSIONS

This work investigated the corrosion behavior of AZ80-xNd alloys in Na_2SiO_3 solution at different pH values with the elimination of the β-$Mg_{17}Al_{12}$ phase by heat treatment. Several conclusions are given as follows:

1. The heat treatment at 410°C for 10 h of AZ80-xNd alloys effectively eliminates the β-$Mg_{17}Al_{12}$ phase, while the left two kinds of Nd-rich phases in the alloys, namely the Al_2Nd phase and AlMnNd phase.
2. Both Al_2Nd and AlMnNd phases have more positive potentials than the Mg matrix, which builds the galvanic couples with the Mg matrix, resulting in the acceleration of the corrosion process, while the AlMnNd phase tends to decompose and provides a protective layer for alloys. When the Nd content is 1.2 wt.%, the alloy shows outstanding corrosion resistance in Na_2SiO_3 solutions with different pH values among the four alloys with different Nd contents.
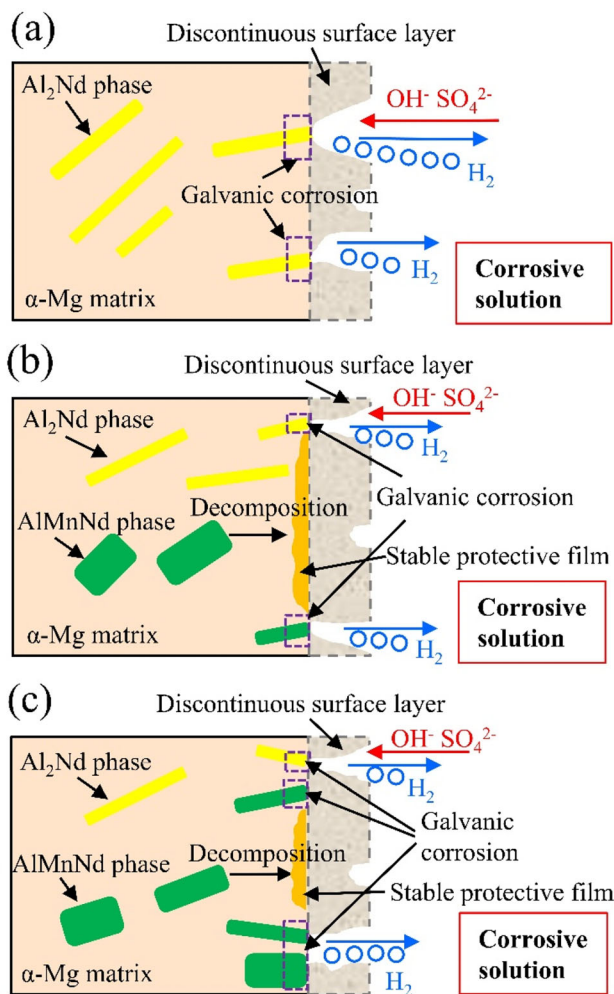
Fig. 8. Schematics of corrosion process: (a) AZ80-0.4Nd alloy (only Al$_2$Nd phase in the alloy); (b) AZ80-1.2Nd alloy; (c) AZ80-1.6Nd alloy.

3. The alloys exhibit better corrosion resistance in the strong alkaline solution than in the weak alkaline solution, due to the slower corrosion rate of the magnesium matrix in the alkaline solution and the decomposition of the AlMnNd phase.

ACKNOWLEDGEMENTS

CONFLICT OF INTEREST

The authors declare no conflict of interest.

SUPPLEMENTARY INFORMATION

The online version contains supplementary material available at https://doi.org/10.1007/s11837-021-04974-7.

REFERENCES

1. Z. Shi, F. Cao, G.L. Song, M. Liu, and A. Atrens, *Corros. Sci.* 76, 98. (2013).
2. M. J. Anjum, J. Zhao, V. Zahedi Asl, G. Yasin, W. Wang, S. Wei, Z. Zhao, W. Qamar Khan, *Corros. Sci.* 157, 1. (2019).
3. A. D. Forero López, I. L. Lehr, L. I. Brugnoni, S. B. Saidman, *J. Magnes. Alloy.* 6, 15. (2018).
4. K. Gusieva, C. H. J. Davies, J. R. Scully, N. Birbilis, *Int. Mater. Rev.* 60, 169. (2014).
5. G. Barati Darband, M. Aliofkhazraei, P. Hamghalam, N. Valizade, *J. Magnes. Alloy.* 5, 74. (2017).
6. H. Huo, Y. Li, and F. Wang, *Corros. Sci.* 46, 1467. (2004).
7. L.M. Calado, M.G. Taryba, M.J. Carmezim, and M.F. Montemor, *Corros. Sci.* 42, 12. (2018).
8. H. Y. Yang, X. B. Chen, X. W. Guo, G. H. Wu, W. J. Ding, N. Birbilis, *Appl. Surf. Sci.* 258, 5472. (2012).
9. S. K. Woo, C. Blawert, K. A. Yasakau, S. Yi, N. Scharnagl, B. C. Suh, Y. M. Kim, B. Sun You, C. Dong Yim, *Corros. Sci.* 166, (2020).
10. L. Yang, X. Zhou, S. M. Liang, R. Schmid-Fetzer, Z. Fan, G. Scamans, J. Robson, G. Thompson, *J. Alloys Compd.* 619, 396. (2015).
11. Z. Zhang, G. Wu, A. Atrens, W. Ding, *J. Magnes. Alloy.* 8, 301. (2020).
12. Y. L. Song, Y. H. Liu, S. R. Yu, X. Y. Zhu, S. H. Wang, *J. Mater. Sci.* 42, 4435. (2007).
13. J. H. Nordlien, *J. Electrochem. Soc.* 144, (1997).
14. S. Mathieu, C. Rapin, J. Steinmetz, and P. Steinmetz, *Corros. Sci.* 45, 2741. (2003).
15. H. Y. Choi, W. J. Kim, *J. Alloys Compd.* 696, 736. (2017).
16. T. Takenaka, T. Ono, Y. Narazaki, Y. Naka, and M. Kawakami, *Electrochim. Acta* 53, 117. (2007).
17. T. J. Lee, W. J. Kim, *J. Alloys Compd.* 617, 352. (2014).
18. N. Liu, J. Wang, L. Wang, Y. Wu, and L. Wang, *Corros. Sci.* 51, 1328. (2009).
19. Y. J. Feng, L. Wei, X. B. Chen, M. C. Li, Y. F. Cheng, Q. Li, *Corros. Sci.* 159, (2019).
20. F. Rosalbino, E. Angelini, S. De Negri, A. Saccone, S. Delfino, *Intermetallics* 13, 55. (2005).
21. X. Chen, Q. Liao, Q. Le, Q. Zou, H. Wang, A. Atrens, *Electrochim. Acta* 348, (2020).
22. W. Liu, F. Cao, L. Chang, Z. Zhang, and J. Zhang, *Corros. Sci.* 51, 1334. (2009).
23. F. Rosalbino, E. Angelini, S. De Negri, A. Saccone, S. Delfino, *Intermetallics* 14, 1487. (2006).
24. R. Arrabal, B. Mingo, A. Pardo, E. Matykina, M. Mohedano, M.C. Merino, A. Rivas, and A. Maroto, *Corros. Sci.* 97, 38. (2015).
25. T. Zhang, G. Meng, Y. Shao, Z. Cui, and F. Wang, *Corros. Sci.* 53, 2934. (2011).
26. M. Su, J. Zhang, Y. Feng, Y. Bai, W. Wang, Z. Zhang, F. Jiang, *J. Alloys Compd.* 691, 634. (2017).
27. J. L. Zhang, Y. L. Liu, J. Zhou, Z.Y. Feng, S. B. Wang, *J. Alloys Compd.* 629, 290. (2015).
28. R. Hay, and C.P. Ostertag, *Corros. Sci.* 153, 213. (2019).

29. J. Williamson, and O.B. Isgor, *Corros. Sci.* 106, 82. (2016).
30. A.D. King, N. Birbilis, and J.R. Scully, *Electrochim. Acta* 121, 394. (2014).
31. M.C. Zhao, M. Liu, G. Song, and A. Atrens, *Corros. Sci.* 50, 2008. (1939).
32. N.D. Nam, W.C. Kim, J.G. Kim, K.S. Shin, and H.C. Jung, *Corros. Sci.* 51, 2942. (2009).
33. H. Zou, X. Zeng, C. Zhai, W. Ding, *Mater. Sci. Eng., A* 392, 229. (2005).
34. N. Jiang, L. Chen, L. Meng, C. Fang, H. Hao, X. Zhang, *J. Rare Earths* 34, 632. (2016).
35. D. Qiu, M.X. Zhang, J.A. Taylor, H.M. Fu, and P.M. Kelly, *Acta Mater.* 55, 2007. (1863).
36. X. Chen, S. Ning, A. Wang, Q. Le, Q. Liao, Y. Jia, C. Cheng, X. Li, A. Atrens, F. Yu, *Corros. Sci.* 163, (2020).
37. N. Wang, R. Wang, C. Peng, Y. Feng, and B. Chen, *Corros. Sci.* 64, 17. (2012).
38. Y. Tian, L.J. Yang, Y.F. Li, Y.H. Wei, L.F. Hou, Y.G. Li, R.I. Murakami, and T. Nonferr, *Metal Soc.* 21, 912. (2011).
39. V. Barranco, S. Feliu, and S. Feliu, *Corros. Sci.* 46, 2221. (2004).
40. M. Anik, and G. Celikten, *Corros. Sci.* 49, 2007. (1878).
41. C. B. Genevie've Baril, and Nadine Pe´be'rez, *J. Electrochem. Soc.* 148, B489. (2001).
42. R. Arrabal, E. Matykina, A. Pardo, M.C. Merino, K. Paucar, M. Mohedano, and P. Casajús, *Corros. Sci.* 55, 351. (2012).
43. R. Arrabal, A. Pardo, M.C. Merino, M. Mohedano, P. Casajús, K. Paucar, and G. Garcés, *Corros. Sci.* 55, 301. (2012).
44. K. A. Unocic, H. H. Elsentriecy, M. P. Brady, H. M. Meyer, G. L. Song, M. Fayek, R. A. Meisner, B. Davis, *J. Electrochem. Soc.* 161, C302. (2014).
45. M. Esmaily, D. B. Blücher, J. E. Svensson, M. Halvarsson, L. G. Johansson, *Scripta Mater.* 115, 91. (2016).
46. G.L. Song, and M. Liu, *Corros. Sci.* 62, 61. (2012).
47. M. Taheri, J.R. Kish, N. Birbilis, M. Danaie, E.A. McNally, and J.R. McDermid, *Electrochim. Acta* 116, 396. (2014).
48. L. Chai, X. Yu, Z. Yang, Y. Wang, and M. Okido, *Corros. Sci.* 50, 3274. (2008).
49. J. Chen, J. Wang, E. Han, J. Dong, and W. Ke, *Electrochim. Acta* 52, 3299. (2007).